Mixture of learners for cancer stem cell detection using CD13 and H and E stained images

Oğuzhan Oğuz, Cem Emre Akbaş, Maen Mallah, Kasım Taşdemir, Ece Akhan Güzelcan, et al.

Oğuzhan Oğuz, Cem Emre Akbaş, Maen Mallah, Kasım Taşdemir, Ece Akhan Güzelcan, Christian Muenzenmayer, Thomas Wittenberg, Ayşegül Üner, A. Enis Cetin, Rengül Çetin Atalay, "Mixture of learners for cancer stem cell detection using CD13 and H and E stained images," Proc. SPIE 9791, Medical Imaging 2016: Digital Pathology, 97910Y (23 March 2016); doi: 10.1117/12.2216113

SPIE.

Event: SPIE Medical Imaging, 2016, San Diego, California, United States

Mixture of Learners for Cancer Stem Cell Detection Using CD13 and H&E Stained Images

Oğuzhan Oğuz[a], Cem Emre Akbaş[a], Maen Mallah[a], Kasım Taşdemir[b], Ece Akhan Güzelcan[c], Christian Muenzenmayer[d], Thomas Wittenberg[d], Ayşegül Üner[e], A. Enis Çetin[a], and Rengül Çetin Atalay[c]

[a]Department of Electrical and Electronics Engineering, Bilkent University, Ankara, Turkey
[b]Department of Computer Engineering, Abdullah Gül University, Kayseri, Turkey
[c]Graduate School of Informatics, Middle East Technical University, Ankara, Turkey
[d]Fraunhofer-Institute for Integrated Circuits IIS, Erlangen, Germany
[e]Cancer Institute, Hacettepe University, Ankara, Turkey

ABSTRACT

In this article, algorithms for cancer stem cell (CSC) detection in liver cancer tissue images are developed. Conventionally, a pathologist examines of cancer cell morphologies under microscope. Computer aided diagnosis systems (CAD) aims to help pathologists in this tedious and repetitive work. The first algorithm locates CSCs in CD13 stained liver tissue images. The method has also an online learning algorithm to improve the accuracy of detection. The second family of algorithms classify the cancer tissues stained with H&E which is clinically routine and cost effective than immunohistochemistry (IHC) procedure. The algorithms utilize 1D-SIFT and eigen-analysis based feature sets as descriptors. Normal and cancerous tissues can be classified with 92.1% accuracy in H&E stained images. Classification accuracy of low and high-grade cancerous tissue images is 70.4%. Therefore, this study paves the way for diagnosing the cancerous tissue and grading the level of it using H&E stained microscopic tissue images.

Keywords: Cancer Stem Cell Detection, CD13 Stain, H&E Stain, Region Covariance Descriptor,Region Codifference Descriptor, Online Learning, 1-D SIFT, Eigenface

1. INTRODUCTION

Histopathological image analysis plays an important role in diagnosing of many illnesses including cancer. Mitotic index, cancer tissue grading, and analysis of metastatic invasion can be acquired from microscopic images with the help of qualified pathologist. Recently developed computer assisted digital pathology systems can help pathologists. By using a proper computer-aided diagnosis (CAD) system, diagnosis time can be significantly reduced. It may also be possible to reduce human based errors.

Pathologists detect and count cancer stem cells (CSC) on tissue images stained with CSC markers such as CD13 antibodies. CD13 stain is one of the marker used to this end. It is perceptually easier to determine the CSCs in microscopic images of the tissues stained with CD13 antibodies by immunohistochemstry. On the other hand staining with CD13 antibodies is costly compared to the routine Hematoxylin and Eosin (H&E) staining. H&E is a routine stain which has been around for more than 100 years. However, its low cost comes with a price. It is perceptually harder to determine CSCs in H&E than CD13 stained tissues.

Further author information: (Send correspondence to O.Oğuz)
O.Oğuz: E-mail: ooguz@bilkent.edu.tr, Telephone: +90-312-290-1219
K. Taşdemir: E-mail: kasim.tasdemir@agu.edu.tr,
C. Muenzenmayer: E-mail: christian.muenzenmayer@iis.fraunhofer.de
A.Üner: E-mail: unera@hacettepe.edu.tr
A.E.Çetin : E-mail: cetin@bilkent.edu.tr
R.Ç.Atalay: E-mail: rengul@metu.edu.tr

Medical Imaging 2016: Digital Pathology, edited by Metin N. Gurcan, Anant Madabhushi, Proc. of SPIE Vol. 9791, 97910Y · © 2016 SPIE
CCC code: 1605-7422/16/$18 · doi: 10.1117/12.2216113

In this paper, algorithms for cancer stem cell (CSC) detection in both CD13 and H&E stained liver tissue images are developed. The first algorithm locates CSCs in CD13 stained liver tissue images using an online learning algorithm by combining several learners. CSCs in CD13 stained tissue images can be automatically identified using region covariance[1] and co-difference[2] descriptors.[3] Our CD13 positive cell detection method has an online decision fusion strategy. Initially, it linearly combines region covariance and co-difference descriptors. Based on the feedback from a pathologist the algorithm updates the weights of individual descriptors. This weight update strategy is similar to the least mean square (LMS) based online decision fusion strategy used in some other image and video processing problems.[4,5]

Since staining with H&E instead of CD13 antibodies is a routine pathological process we propose two texture analysis based image classification algorithms for H&E stained images of liver tissues. Our algorithms analyze H&E images using one-dimensional Scale Invariant Feature Transform (1-D SIFT) features and eigenvectors of the image covariance matrices to classify them as normal, low-grade and high-grade cancer tissue images. 1-D SIFT method is inspired by the well-known 2-D SIFT algorithm.[6] The latter is a classification algorithm similar to the conventional eigenface algorithm.[7]

The outline of this paper is as follows. In Section 2 detection process of CSCs in CD13 images is described and experimental results are presented. Section 3 explains the classification of H&E images by using 1-D SIFT algorithm. In Section 4 the same classification problem is addressed and solved using the eigen-analysis based method. Normal and cancerous tissues can be classified with 92.1% accuracy in H&E stained images in our database. Classification accuracy of low and high-grade cancer tissue images is 70.4%.

2. MIXTURE OF ONLINE LEARNERS FOR CANCER STEM CELL DETECTION IN CD13 STAINED MICROSCOPIC IMAGES

Pathologists can detect cancer stem cells from immunohistochemical cancer tissue slides stained with CD13 marker under the microscope. The microscopic images of CSCs and cancer cells appear as dark brown and blue respectively. These regions are indicated in Figure 1. Pathologists needs to identify the CSCs to determine the severity of the cancer. Our purpose is to make this processes quantitatively significant and reduce human based errors. Our algorithm linearly combines the results of region covariance and region co-difference algorithms, and displays CSC marked regions to the pathologist. Since the tissue microarray (TMA) images are large, only a small portion of the tissue is displayed on the monitor. If the pathologists want to correct the automatically marked regions, they mark incorrectly determined CSC regions and/or undetected CSC regions on the screen using the cursor of mouse. Based on the feedback from the pathologists, weights of the individual learners are updated using an LMS (Least Mean Square) based online learning algorithm. Then, the entire tissue image is marked and quantified again using the updated weights.

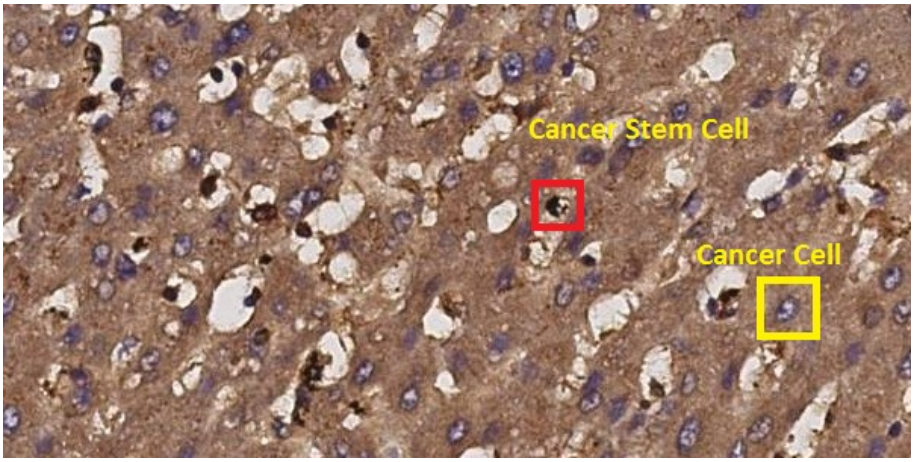

Figure 1. Immunohistochemistry (IHC) images of liver cancer tissue stained using CD13 primary antibodies.

2.1 Feature Extraction

We used region covariance and region co-difference descriptors to represent the image regions . The region covariance method for feature extraction is well-studied for human and object detection in images[1,8–11] . It is shown that using the covariance matrix in the classification applications gives reliable results than the other approaches.[9] The region co-difference method is the modified version of it[2]. It mitigates the cost problem stems from multiplication operation by using a novel vector product definition. Instead of a conventional multiplication, a multiplication-free operation is implemented. In the region co-difference method, the co-difference matrix is used as a region descriptor. It is employed in various applications[3,12].

A feature vector is extracted from each pixel and used in construction of the region covariance and the co-difference matrices. The feature vectors are extracted from overlapping windows of size 11x11 pixels. The structure of the feature vector is:

$$f_k = \left[R(x,y), \quad G(x,y), \quad B(x,y), \quad \frac{dR(x,y)}{dx}, \frac{dR(x,y)}{dy}, \quad \frac{d^2R(x,y)}{dx^2}, \quad \frac{d^2R(x,y)}{dy^2}\right] \tag{1}$$

where $R(x,y)$, $G(x,y)$ and $B(x,y)$ are the pixel values at (x,y) positions in red, green and blue channels, respectively. The last four elements of the feature vector are the first and second derivatives of the red channel with respect to x and y. Covariance matrix, C_V, is derived from the extracted feature vector as in Equation 2:

$$C_V = \frac{1}{N-1}\sum_{k=1}^{N}(f_k - \bar{\mu}) \times (f_k - \bar{\mu})^T \tag{2}$$

In Equation 2, N is the number of pixels. This is 121 for given a 11x11 window. The mean vector, $\bar{\mu}$, is defined as follows:

$$\bar{\mu} = \left[0, \quad 0, \quad 0, \quad \mu(\frac{dI_R}{dx}), \quad \mu(\frac{dI_R}{dy}), \quad \mu(\frac{d^2I_R}{dx^2}), \quad \mu(\frac{d^2I_R}{dy^2})\right] \tag{3}$$

where I_R represents the image pixels in the red channel. The mean operation, $\mu : \mathbb{Z}^2 \rightarrow \mathbb{Z}$, takes mean of given pixels. The extracted mean values are kept as a vector $\bar{\mu}$. The first three elements of $\bar{\mu}$ are taken as zero in order to preserve the pixel color information after the extraction in Equation 2. Although the calculation cost of a single covariance matrix is not too high, as the number of covariance matrices increase, it will escalate. By using the co-difference matrix presented in Equation 4 reduces this cost[2] :

$$C_D = \frac{1}{N-1}\sum_{k=1}^{N}(f_k - \bar{\mu}) \oplus (f_k - \bar{\mu})^T \tag{4}$$

The operator $\oplus$ is defined in[2] as an additive operator which is used instead of the scalar multiplication used in Equation 2. Loosely speaking, it behaves like a matrix multiplication operation. Even $\oplus$ is an addition operation. Due to sign of the of the outcome, it acts like a multiplication operation. The operation $\oplus$ between real numbers a and b is defined as in Equation 5. For the further details see.[2]

$$a \oplus b = \text{sign}(a \text{ x } b)(|a| + |b|) \tag{5}$$

$$C_{ROI} = \begin{bmatrix} C_{1,1} & \cdots & C_{1,7} \\ \vdots & \ddots & \vdots \\ C_{7,1} & \cdots & C_{7,7} \end{bmatrix} \tag{6}$$

In Equation 6, C_{ROI} represents the calculated C_V or C_D matrices. In Equation 6, only the lower triangle values are taken into account because of the symmetry. The values of the lower triangle part are placed into a vector with the size of 1 x 28. The regions are represented with this z_k vector:

$$z_k = [C_{1,1}, C_{2,1}, C_{2,2}, C_{3,1}, C_{3,2}, C_{3,3} \cdots, C_{7,6}, C_{7,7}] \tag{7}$$

In addition to the region covariance and the co-difference descriptors, mean values of R, G, B, Y, Cb, Cr, H ,S, V, channels are also extracted from corresponding 11x11 windows and used as a feature vectors. To sum up, from a 11x11 window we extract five feature vectors: z_k's for both the covariance and the co-difference region descriptors and three separate mean value feature vectors corresponding each color space.

2.2 Mixture of Learners (MoL) Algorithm

Mixture of Learners (MoL) method combines the trained machine learning models to achieve the best CSC classification in CD13 images. First, the entire image is scanned with an overlapping window of size 11 x 11 pixels. The feature vectors mentioned in Section 2.1 are obtained from these windows. The size of the feature vector depends on the region description method. These feature vectors of the same type are concatenated to construct a feature matrix which represents the whole image. Therefore, five different feature matrices are constructed for a single image. Each row of this matrices are fed into the learners shown as Learner N in Figure 2. The predictions, $L_p(n), n \in (1, ..., N)$, for each window are obtained separately. $L_p(n)$ is one for positive detection and minus one for otherwise. In our implementation we have ten learners, thus the number of maximum learner N is 10.

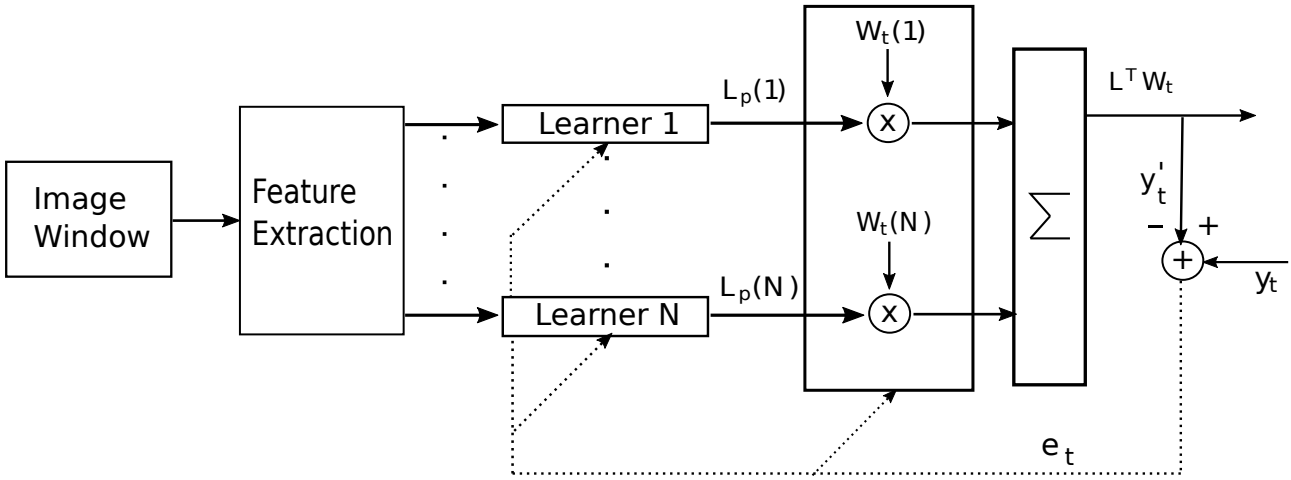

Figure 2. Mixture of learners block diagram.

In Figure 2, the block diagram of MoL algorithm is presented. In the MoL algorithm, the feature vectors are extracted from the image windows and fed into the related prediction model. Prediction results of the each model are multiplied with an initial weight vector W_t and then linearly combined as $L^T W_t$. After the first run, the predicted image is shown to the user via Graphical User Interface (GUI). The user indicates the incorrectly marked regions with a marking tool in the GUI. According to this feedback y_t of the user, the system updates the weights, W_t, of individual learners. A gradient descent type algorithm is used to update the weights as:

$$W_{t+1} = W_t + \frac{e_t}{\|L\|^2} L \tag{8}$$

where $W_{t+1} = [w_{t+1,1}, \ldots, w_{t+1,10}]^T$ is the updated weight vector at time $t+1$, $W_t = [w_{t,1}, \ldots, w_{t,10}]^T$ is the current weight vector at time t. L is the decision vector of the learners defined as $L = [L_p(1), L_p(2), \ldots, L_p(10)]$ and e_t is the loss (or error) which is defined as :

$$e_t = y_t - y'_t \tag{9}$$

where the y'_t is the current predicted value calculated from $L^T W_t$ as shown in Figure 2. The algorithm works with the updated weights and repeats until the user decides to stop this process.

In some cases the weight update process fails to classify some regions as indicated by the user. In order to achieve the desired output, we expand L_t with additional information. The additional information represents a distance measure between that region and all regions in the image. The distance between two regions is calculated using co-difference values as in[12]:

$$d(C_1, C_2) = \sum_{i=1}^{p} \left[\sum_{j=1}^{p} \frac{|C_1(i,j) - C_2(i,j)|}{(C_1(i,i) + C_2(i,i))} \right] \tag{10}$$

After the distances between the desired -could not be classified correctly region- and all regions are calculated, a sigmoid function is used to map the distances to values (v) between 0 and 1.

$$sigm(d) = \frac{1}{1 + e^{-a(x-c)}} \tag{11}$$

where $c = 0.5$ and $a = -8$.

However, the desired region could be *not a CSC* (label : -1) or *CSC* (label : 1) region. Thus, v is multiplied by the desired label to indicate the class information. This information is then added to the decision vector L. The new column added to L and a weight that is independent from the weight update process is assigned to it. Moreover, the co-difference values of the desired -could not be classified correctly region- are saved along with the desired label. This is necessary to be able to compute the distances when another image is used as input to the system.

2.3 Experimental Setup and Results

The serial sections of TMA samples of liver cancer were purchased from US BioMAX (http://www.biomax.us/tissue-arrays). The paraffin embedded TMA tissues were deparaffinized and stained with Dako EnVision kit using CD13 primary antibodies in 1:500 dilutions. Finally immunohistochemistry stained TMA samples analyzed under light microscope (EUROMEX-Oxion). The images which are utilized in ground truth data extraction are in 20X magnification with the size 600x600 pixels. Our CSC data set constructed as follows: In total 840 windowed regions from seven CD13 images are taken both for CSC and other image regions. Images are normalized between [0,1]. Since the co-difference operation is a non-linear operation, it causes loss of information after the normalization. Therefore, the normalization is applied for all feature extraction cases except for the co-difference case. In Support Vector Machines (SVM), Radial Basis Function (RBF) kernel and 5-fold cross validation is applied by using LiBSVM tool.[13] Best parameters for RBF kernel such as C and γ are selected via grid search. Neural Networks (NN) are built with the MATLAB®'s Artificial Neural Networks (ANN) application for pattern recognition. The number of hidden layers in the NN are taken as 10 and *scaled conjugate gradient back propagation* is used. We divide 60% of our data for training, 20% for cross-validation and 20% for the test phase.

Table 1. SVM Model Information of the Region Descriptors.

Method	Accuracy (%)
Covariance SVM	97.61
Co-Difference SVM	98.08
RGB-Mean SVM	98.21
YCbCr-Mean SVM	95.83
HSV-Mean SVM	97.61

Table 2. Neural Network Model Information of the Region Descriptors.

Method	Accuracy (%)	Cross Entropy
Covariance NN	97.00	2.97461
Co-Difference NN	96.40	1.68052
RGB-Mean NN	98.20	2.17499
YCbCr-Mean NN	97.00	2.63928
HSV-Mean NN	98.80	2.15902

Accuracies of the trained models in the training set are shown in Tables 1 and 2. To measure the test quality and test accuracy Matthews Correlation Coefficient (MCC)[14] and F1 score[15] is used respectively. MCC is a balanced measure for binary classification. Correlation between the observed and the predicted classification is calculated by using MCC. It defined on [-1,1], where one represents perfect correlation and minus one means no correlation. MCC is calculated as follows:

$$MCC = \frac{(TP)(TN) - (FP)(FN)}{\sqrt{(TP+FP)(TP+FN)(TN+FP)(TN+FN)}} \tag{12}$$

where TP, TN, FP and FN stands for true positive, true negative, false positive and false negative respectively. Balanced F1 $\in [0,1]$ measure is a harmonic mean of precision and recall. It is used for measuring the test accuracies. F1 score defined as:

$$F1 = 2 \times \frac{Precision \times Recall}{Precision + Recall} \tag{13}$$

where precision and recall is defined as:

$$Precision = \frac{TP}{TP+FP} \tag{14}$$

$$Recall = \frac{TP}{TP+FN} \tag{15}$$

Table 3. Average Classification Results.

Method	MCC	F1	Specificity	Recall	Precision
Co-Difference SVM	0.2916	0.2720	0.9743	0.3019	0.4219
Covariance SVM	0.4175	0.3883	0.9757	0.4062	0.5774
Co-Difference NN	0.3444	0.2977	0.9964	0.2164	0.6581
Covariance NN	0.2251	0.2298	0.9510	0.3750	0.1798
RGB-Mean SVM	0.4463	0.4255	0.9605	0.5155	0.5074
RGB-Mean NN	0.4090	0.3622	0.9947	0.2858	0.7216
YCbCr-Mean SVM	0.4407	0.4173	0.9654	0.4843	0.5316
YCbCr-Mean NN	0.4341	0.4024	0.9913	0.3513	0.6619
HSV-Mean SVM	0.4278	0.3961	0.9892	0.3546	0.6471
HSV-Mean NN	0.4046	0.3636	0.9935	0.2941	0.6987
Initial Weight Combination Result	0.4586	0.4369	0.9875	0.4117	0.6153
User Guided Result	0.6330	0.6284	0.9787	0.7997	0.5232

Individual learner results are shown in Table 3. The values in Table 3 are the average classification results of 19 CD13 images. Initial weight combination result indicates the first combined outcome with the initial weights. User Guided Result row in Table 3 shows the results of the updated system after the user feedbacks.

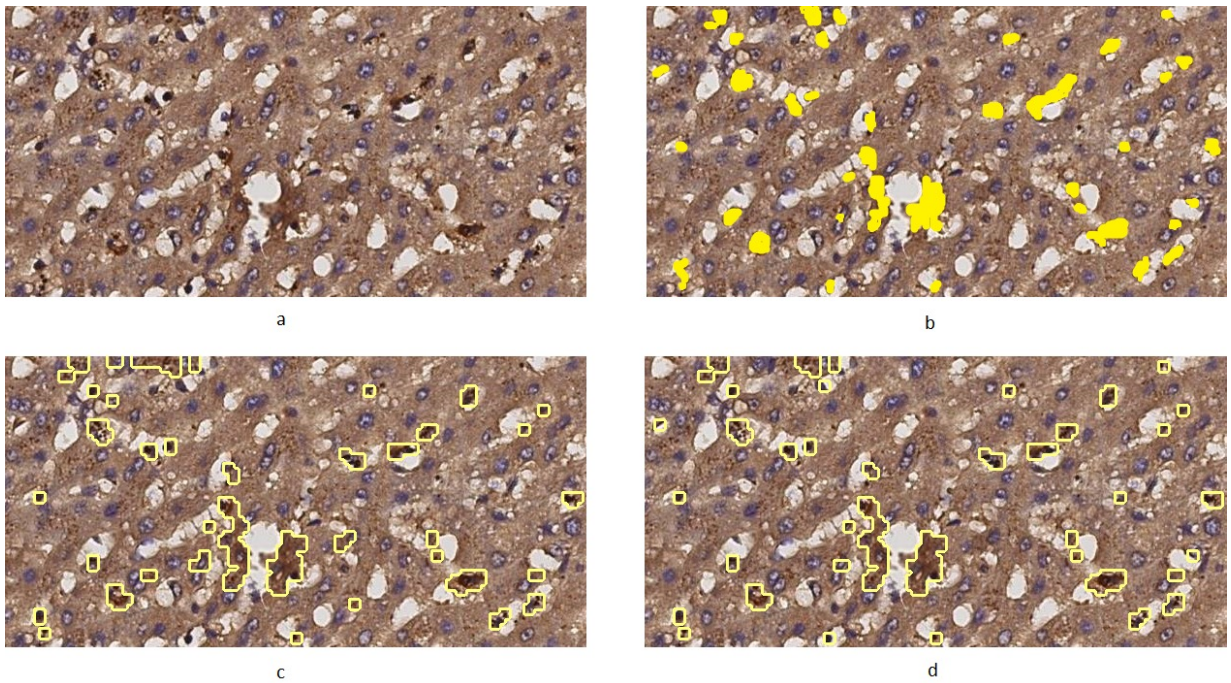

Figure 3. A CD13 stained image (a), its ground truth image marked by pathologist (b), first result of the MoL algorithm (c), achieved result after user feedbacks (d).

An output of the proposed algorithm is demonstrated in Figure 3. A CD13 image given in Figure 3 (a) is fed to the learning algorithm. The ground-truth labels are shown in Figure 3 (b). The output obtained with the initial weights is shown in Figure 3 (c). The miss-detected regions can be observed in 3 (c). In Figure 3 (d), result obtained from the updated system with the user feedbacks is presented. It is evident from the figure that number of miss detected regions are decreased.

3. CLASSIFICATION OF H&E IMAGES BY USING 1-D SIFT METHOD

H&E stain is a cost effective routine histopathological technique.[16–20] Unlike CD13 images, it is difficult to distinguish CSCs in H&E images. CSCs appear in dark brown colors and can be easily noticed in a CD13 stained image. Thus, a method which can classify H&E images according to CSC densities would make this process cheaper and more accessible. The aim of this section is to present an algorithm to classify H&E images according to their CSC densities.

Before presenting the algorithm, it is necessary to briefly explain the relative parts of acquisition of these microscopic images from the patients. First, a sample tissue is taken from the patient and it is finely sliced in very thin layers (tissue sections). The adjacent sections looks very similar but actually they are not exactly the same layer. Subsequently, the sections are stained with either H&E or CD13 stain. Note that an already stained section cannot be stained again with another dye/marker. For that reason, it is not possible to have both CD13 and H&E stained images of exactly the same tissue section. To overcome this problem, adjacent sections of the same tissue are stained with different stains assuming that they have similar cancer properties. Based on this assumption, CSC density calculated on a CD13 stained section image is associated with its adjacent layer which is stained with H&E. Therefore, ground truth information for H&E images is created.

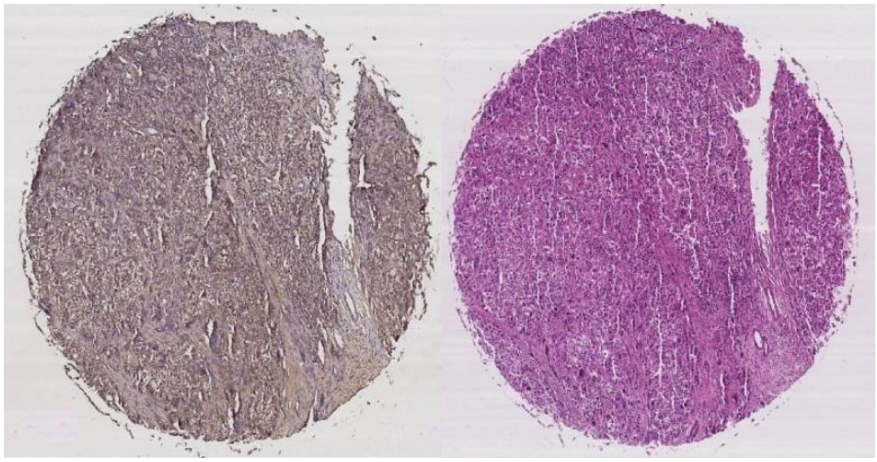

Figure 4. CD13 (left) and H&E (right) stained serial section tissue images of the same patient.

In Figure 4, the adjacent sections for the same tissue are shown. Various collocating regions of these images are chosen. CSC density in the chosen regions are calculated as a percentage of CSCs to all cells. This process is carried out on the chosen image region of CD13 stained tissue. The calculated density also gives that of corresponding H&E region. The ratio which gives us the CSC density in the chosen region is as follows:

$$CellRatio = \frac{\sum CSC}{\sum AllCells} \times 100 \tag{16}$$

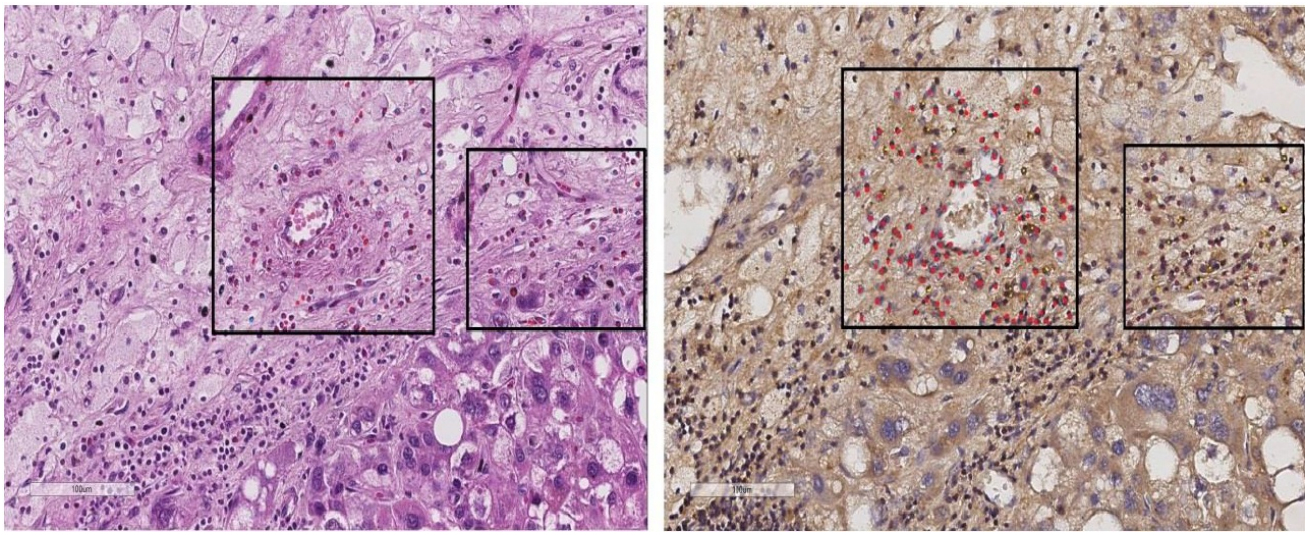

Figure 5. Corresponding regions of H&E (left) and CD13 (right) stained tissue images.

According to this ratio, a grading scheme is defined. If the Cell Ratio is less than 5%, that region is considered to have a low-grade and labeled as Grade-I. If it is greater or equal to 5%, it is labeled as a Grade-II meaning that it is a high-grade cancer region. It is noteworthy to remind that CD13 images are only used for labeling H&E images. They are not involved in the training stage in any means at all.

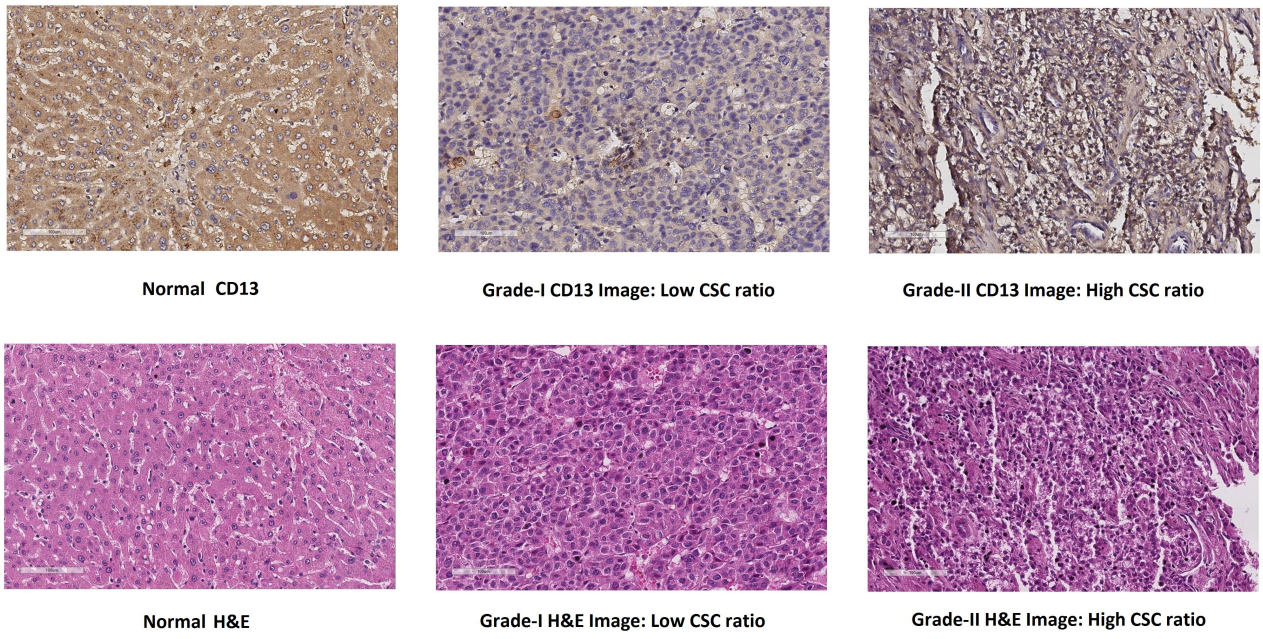

Figure 6. CD13 and H&E image examples according to estimated CSC levels.

In Figure 6 example images for normal, Grade-I and Grade-II are shown. These H&E images are fed into the

1-D SIFT algortihm, which is explained in the following Section 3.1.

3.1 1-D SIFT Algortihm

In[21] , 1-D SIFT algorithm is presented. It is inspired from famous SIFT[6] algorithm and utilized in merging super pixels. However, steps like key point detection, feature vector extraction and matching are disregarded. In this work, 1-D SIFT algorithm is expanded to incorporate these steps and applied to an image classification problem.

In SIFT[6] , identical key points are extracted from 2-D images. 1-D SIFT algorithm extracts the key points from the images color histograms. As in 2-D SIFT method, 1-D histograms are filtered with 1-D difference of Gaussian filters. Then, local extrema and minima locations are determined. Footprints of these extrema and minima points are backtracked from the lowest scale to the highest scale. If it is able to backtrack an extrema or a minima location from coarsest level to the highest level, that location is taken as a key point. After the key point indexes are found, gradient of the color histogram is calculated. 8 neighboring gradient values around the key points are taken. According to their magnitudes, they placed into a feature vector.

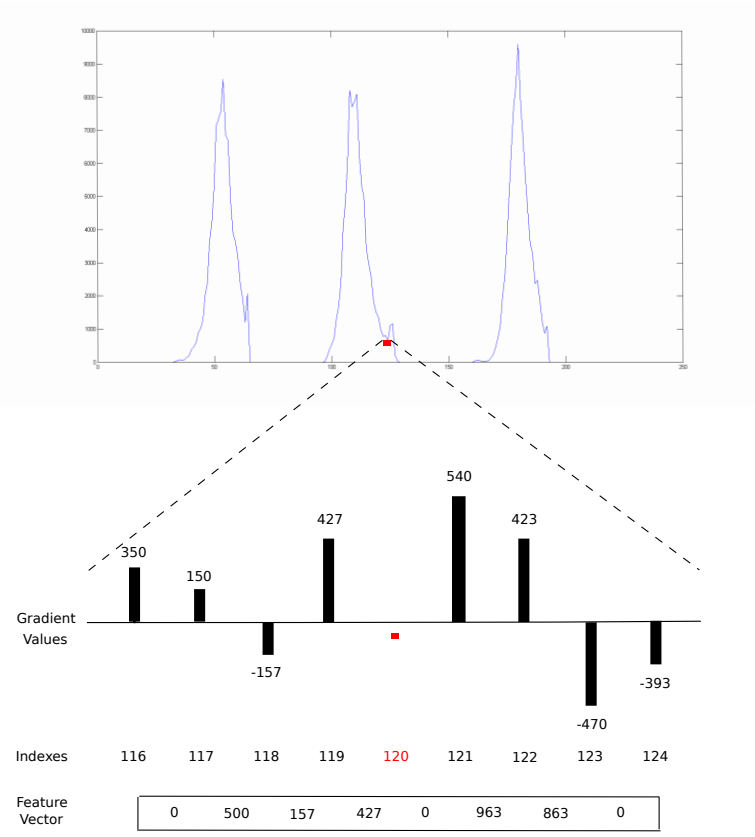

Figure 7. Feature Vector Extraction in 1-D SIFT Algorithm.

In Figure 7, feature vector extraction process for 1-D SIFT algorithm is graphically explained. A key point location is shown with a red dot on 32-binned RGB histogram at index 120. Gradient values are paired together and according to their signs and their magnitudes placed into feature vector. The negative values are summed and inserted into the first element where positive ones are also summed and placed into second element of the

feature vector. Thus, a feature vector with four pairs is constructed. This process is applied to the all images in our data set.

3.2 Experimental Results

Serial sections of the same TMA samples stained with CD13 were deparaffinized and stained with Hematoxylin (Harris Hematoxylin)/Eosin-phloxine according to manufacturers protocol (Harris). H&E stained TMA samples analyzed under light microscope (EUROMEX-Oxion) and images are acquired with 20X objectives. Our image data set contains 454 H&E stained liver images which taken from 56 different patients. 184 of these samples are from healthy patients and the other 270 images are taken from the patients diagnosed with cancer. According to our grading ratio defined in Equation 16, 119 out of 270 are labeled as Grade-I and tile size of the images chosen as 300x300 pixels.

Several experiments are conducted in order to find the best way for the classification process. Since we don't have only one image for each patient, in each experiment, we follow leave one person out approach. First, we focus on differentiating normal images from cancerous images.

In our first experiment, Principal Component Analysis (PCA) based feature vectors is used. The first eigenvectors are taken and fed into k-NN algorithm. Number of neighbors k is taken as three. As a second experiment, the weighted combination of the first four eigenvectors and their linear combinations are computed. Best classification accuracy is obtained when five times of the first eigenvector is combined with the third eigenvector itself. Lastly, matching algorithms presented in Section 7.1 and 7.2 of SIFT[6] are carried out. In section 7.1 of,[6] for each key point, a ratio between the distances of the first and second closest key point matches is calculated. The key points with ratio larger than 0.8 are disregarded. In section 7.2 of[6] Best Bin First (BBF) algorithm is used for key point matching. An image classification is concluded after applying majority voting decision rule on key point matches.

Table 4. Cancer vs Normal Image Classification Accuracies of Conducted Experiments.

Experiment	Unnormalized (%)	Normalized (%)
PCA	79.30	77.53
PCA Linear Combination	78.63	81.50
Keypoint Matching (Section 7.1)	86.50	82.81
Efficient Nearest Neighbor Indexing	86.56	82.81

In Table 4, classification accuracies of conducted experiments are presented. In the normalized case, feature vector entities are normalized by dividing each element L_2 norm of the feature vector. These experiments are carried out on feature vectors extracted from RGB histogram. To observe the effect of the different color spaces in our classification problem, similar experiments are applied for both HSV and YCbCr color histograms. To be consistent with the SIFT algorithm[6] , only the Keypoint Matching and the Efficient Nearest Neighbor Indexing (BBF) experiments are taken into consideration.

Table 5. Cancer vs Normal Image Classification Accuracies of Conducted Experiments in Different Color Spaces with Unnormalized Feature Vectors.

Experiment (Unnormalized)	HSV (%)	YCbCr (%)	RGB (%)
Keypoint Matching	88.54	89.86	86.50
Efficient Nearest Neighbor Indexing	88.54	89.86	86.50

Table 6. Cancer vs Normal Image Classification Accuracies of Conducted Experiments in Different Color Spaces with Normalized Feature Vectors.

Experiment (Normalized)	HSV (%)	YCbCr (%)	RGB (%)
Keypoint Matching	85.02	81.27	82.81
Efficient Nearest Neighbor Indexing	85.02	81.27	82.81

As it can be seen from Tables 5 and 6, in feature vector extraction stage, using different color space histograms has a positive effect on classification results. Also applying normalization on the extracted feature vectors affects the accuracies of the classification results negatively. Experiments are expanded by combining different color channels. Since YCbCr color domain gives the best classification results so far, channels of HSV and RGB color domains are combined with YCbCr color histogram.

Table 7. Constructed Combinations with Different Color Domains. Experiments are conducted with Keypoint Matching.

Combination	Unnormalized (%)	Normalized (%)
YCbCr+H	89.42	81.27
YCbCr+S	90.08	79.73
YCbCr+V	90.52	81.27
YCbCr+V+R	89.20	78.41
YCbCr+V+G	90.96	80.39
YCbCr+V+G+S	89.86	79.95
YCbCr+V+G+H	87.44	79.07
YCbCr+V+G+B	90.74	80.39
YCbCr+HSV+RGB	89.42	80.39

Table 8. Constructed Combinations with Different Color Domains. Experiments are conducted with Efficient Nearest Neighbor Indexing (BBF).

Combination	Unnormalized (%)	Normalized (%)
YCbCr+H	89.42	81.27
YCbCr+S	90.30	79.51
YCbCr+V	90.74	81.05
YCbCr+V+R	89.20	78.63
YCbCr+V+G	90.96	80.83
YCbCr+V+G+S	90.08	80.17
YCbCr+V+G+H	87.44	79.07
YCbCr+V+G+B	90.74	80.61
YCbCr+HSV+RGB	89.42	80.39

As it is shown in Tables 7 and 8 using YCbCr+V+G color histogram combination gives the best classification accuracy in classification of normal and cancerous images.

Table 9. Confusion Matrix of YCbCr+V+G Case.

Class	Normal	Cancerous
Normal	147	37
Cancerous	4	266

Table 10. Grade-I vs Grade-II: Confusion Matrix of YCbCr+V+G Case .

Class	Grade-I	Grade-II
Grade-I	20	99
Grade-II	34	117

Table 11. Confusion Matrix of YCbCr+V+G Case in Three Class.

Class	Normal	Grade-I	Grade-II
Normal	173	2	9
Grade-I	17	20	82
Grade-II	27	27	97

In Table 9, confusion matrix of the YCbCr+V+G case is given. Since the best classification result is achieved with YCbCr+V+G combination, in classification of Grade-I and Grade-II images the same combination is used. However, with the chosen color histogram combination we achieve 51% classification accuracy. In Tables 10 and 11 confusion matrices of related problem is shown. Even if it can distinguish normal from cancerous tissue images, 1-D SIFT algorithm fails to differentiate between Grade-I and Grade-II images.

4. CLASSIFICATION WITH MODIFIED EIGENFACE METHOD USING COLOR SPACE FEATURES

In this section, a classification algorithm similar to well-known eigenface algorithm is developed. Unlike conventional eigenface algorithm; instead of pixel values, covariance matrix of color histograms are fed into the eigenface algorithm. Histograms of the image, that of thresholded image, first and second order discrete derivative of them in various color spaces are used to construct the feature matrix. Our feature matrix is as follows:

$$\begin{aligned} F = [&hist(R) \quad hist(R_t) \quad hist(G) \quad hist(G_t) \quad hist(B) \quad hist(B_t) \quad hist(Y) \\ &hist(Y)' \quad hist(Y_t) \quad hist(U) \quad hist(U)' \quad hist(U)'' \quad hist(V) \quad hist(V)' \\ &hist(V)'' \quad hist(H) \quad hist(H_t) \quad hist(E) \quad hist(S) \quad hist(S_t)]^T \end{aligned} \tag{17}$$

where R is red channel, G is green channel, B is blue channel of RGB space respectively; Y is luminance channel, U and V are chrominance channels of YUV space respectively; H is Hematoxylin channel, E is Eosin channel of HE space[17] respectively and S is saturation channel of HSV space. The $hist(.)'$ function denotes the first order discrete derivative of $hist(.)$, $hist(.)''$ function denotes the second order discrete derivative of $hist(.)$ and $(_t)$ denotes pixel thresholding at a specified channel. Pixel thresholding is utilized to extract more descriptive features from darker regions*. In the experiments, this threshold is empirically selected as 200. In R, G, B, Y, U, V and E channels, pixel values greater than 200 are discarded. However, in H and S channels, pixel values smaller than 200 are discarded. Therefore, more representative features of "darker regions" are extracted. In Equation 17, $hist(.)$ function produces a column vector of size 128×1 in the range (0,255), which leads to a feature matrix F of size 19x128 for each image.

In the proposed modified eigenface method, average covariance matrix of training set is calculated as follows:

$$C_V = \frac{1}{N} \sum_{i=1}^{N} F_i^T \times F_i \tag{18}$$

where N is the number of images in training set and F_i is the feature matrix of i^{th} image. Covariance matrix (C_V) of training set images is a 128x128 matrix. Eigenvalues λ_k and eigenvectors $\boldsymbol{u_k}$ of C_V are computed. The steps below are followed for comparing two images:

(i) Let $\boldsymbol{\gamma}$ be average of columns of $F_m^T \times F_m$ and $\boldsymbol{\zeta}$ be average of columns of $F_n^T \times F_n$,where m is index of the reference image and n is index of the compared image.

(ii) The reference image is projected onto "cell space" by multiplying $\boldsymbol{\gamma}$ with the first 60 vectors of $\boldsymbol{u_k}$ (60 eigenvectors corresponding to 60 largest eigenvalues), as in Equation (19) where $\mu_{\boldsymbol{\gamma}}$ is the mean of $\boldsymbol{\gamma}$.

$$v_k = \boldsymbol{u_k}^T(\boldsymbol{\gamma} - \mu_{\boldsymbol{\gamma}}), k = 1, 2, ..., 60 \tag{19}$$

*Adjectives dark and bright are defined according to RGB color space.

Similarly, the compared image is projected onto "cell space" by multiplying $\boldsymbol{\zeta}$ with the first 60 vectors of $\boldsymbol{u_k}$ (60 eigenvectors corresponding to 60 largest eigenvalues), as in Equation (20) where $\mu_{\boldsymbol{\zeta}}$ is the mean of $\boldsymbol{\zeta}$.

$$w_k = \boldsymbol{u_k}^T(\boldsymbol{\zeta} - \mu_{\boldsymbol{\zeta}}), k = 1, 2, ..., 60 \tag{20}$$

(iii) The distance between two images is defined as follows:

$$d(I_1, I_2) = ||\boldsymbol{v} - \boldsymbol{w}||^2 = \sum_{k=1}^{60}(v_k - w_k)^2 \tag{21}$$

4.1 Experimental Results

The same data space in Section 3 is used in the following experiments. 3-Nearest neighbor classification is used to determine the class of a test image. Similar to Section 3, leave-one-patient-out approach is used. Since a patient has more than one image, the term 'patient classification accuracy' is defined in order to make a decision about patients. In order to classify a patient, majority voting is employed among the decisions of the patient's images.

Table 12. Confusion Matrix of 3-Class 3-NN Eigenface Image Classification

	Grade-I	Grade-II	Normal	Prevelance
Grade-I	70/119	41/119	8/119	58.8%
Grade-II	38/151	102/151	11/151	67.5%
Normal	12/184	5/184	167/184	90.8%
Accuracy	58.3%	68.9%	89.8%	Overall Accuracy 74.7%

Table 13. Confusion Matrix of 3-Class 3-NN Eigenface Patient Classification

	Grade-I	Grade-II	Normal	Prevelance
Grade-I	11/17	5/17	1/17	64.7%
Grade-II	3/17	12/17	2/17	70.6%
Healthy	0/9	0/9	9/9	100%
Accuracy	78.6%	70.6%	75.0%	Overall Accuracy 74.4%

As seen in Table 12, Grade-I and Grade-II images can be classified more accurately than 1-D SIFT based approach does.

Table 14. Confusion Matrix of 2-Class (Normal vs. Cancer) 3-NN Eigenface Image Classification

	Cancerous	Normal	Prevelance
Cancerous	252/270	18/270	93.3%
Normal	18/184	166/184	90.2%
Accuracy	93.3%	90.2%	Overall Accuracy 92.1%

As it is shown in Table 14, 92.1% classification accuracy is achieved when only classifying the images either as cancerous or not . In other words, when Grade-I and Grade-II classification is not required, the classification accuracy of this method is high.

When normal cell images are excluded from the dataset (Table 16), overall Grade-I vs. Grade-II classification accuracy increases to 70.4%. Since the majority voting is employed in patient accuracy calculation, the patient accuracy rate is either equal to or greater than image classification accuracy rate of corresponding case.

Table 15. Confusion Matrix of 2-Class (Normal vs. Cancer) 3-NN Eigenface Patient Classification

	Cancer	Normal	Prevelance
Cancer	31/34	3/34	91.2%
Normal	0/0	9/9	100%
Accuracy	100%	75.0%	Overall Accuracy 93.0%

Table 16. Confusion Matrix of 2-Class (Grade-I vs. Grade-II) 3-NN Eigenface Image Classification

	Grade-I	Grade-II	Prevelance
Grade-I	77/119	42/119	64.7%
Grade-II	38/151	113/151	74.8%
Accuracy	67.0%	72.9%	Overall Accuracy 70.4%

Table 17. Confusion Matrix of 2-Class (Grade I vs. Grade II) 3-NN Eigenface Patient Classification

	Grade-I	Grade-II	Prevelance
Grade-I	11/17	6/17	64.7%
Grade-II	3/17	14/17	82.4%
Accuracy	78.6%	70.0%	Overall Accuracy 73.5%

5. CONCLUSION

In this article CSC detection algorithms in CD13 and H&E stained liver tissue images are developed. CSCs regions are clearly visible in CD13 images. An online learning algorithm which has the capability of accepting feedback from users can achieve very high detection rates in CD13 images. In the second part of the paper we investigated if H&E staining can be used to estimate the CSC levels in liver tissue images or not. It is well-known that it is not possible to observe CSCs in H&E stained tissue images. However, textural structure of the liver tissue images change due to CSCs. Therefore image texture analysis methods can be used to classify H&E stained liver images. It is experimentally shown that it may be possible to estimate the CSC level from the H&E images. With the use of 1-D SIFT and the modified eigen-analysis algorithms it is possible to achieve high recognition rates in normal and cancerous H&E liver tissue images. At this point, our CSC level estimation results are relatively low. Our classification accuracy of high and low CSC level tissue images is about 70%. It is conjectured that it may be possible to increase the CSC level estimation accuracy in the near future.

6. ACKNOWLEDGMENTS

This project is funded by TÜBİTAK with the grant number 213E032.

REFERENCES

[1] Tuzel, O., Porikli, F., and Meer, P., "Region covariance: A fast descriptor for detection and classification," in [*Computer Vision–ECCV 2006*], 589–600, Springer (2006).

[2] Tuna, H., Onaran, I., et al., "Image description using a multiplier-less operator," *Signal Processing Letters, IEEE* **16**(9), 751–753 (2009).

[3] Oguz, O., Muenzenmayer, C., Wittenberg, T., Uner, A., Cetin, A. E., and Atalay, R. C., "Detection of cancer stem cells in microscopic images by using region covariance and codifference method," in [*Computational Intelligence for Multimedia Understanding (IWCIM), 2015 International Workshop on*], 1–5, IEEE (2015).

[4] Yarkan, S., Töreyin, B. U., Qaraqe, K., et al., "An online adaptive cooperation scheme for spectrum sensing based on a second-order statistical method," *Vehicular Technology, IEEE Transactions on* **61**(2), 675–686 (2012).

[5] Günay, O., Töreyin, B. U., and Cetin, A. E., "Online adaptive decision fusion framework based on projections onto convex sets with application to wildfire detection in video," *Optical Engineering* **50**(7), 077202–077202 (2011).
[6] Lowe, D. G., "Distinctive image features from scale-invariant keypoints," *International journal of computer vision* **60**(2), 91–110 (2004).
[7] Turk, M. and Pentland, A., "Eigenfaces for recognition," *J. Cognitive Neuroscience* **3**, 71–86 (Jan. 1991).
[8] Mendez, A. J., Tahoces, P. G., Lado, M. J., Souto, M., and Vidal, J. J., "Computer-aided diagnosis: Automatic detection of malignant masses in digitized mammograms," *Medical Physics* **25**(6), 957–964 (1998).
[9] Porikli, F., Tuzel, O., and Meer, P., "Covariance tracking using model update based on lie algebra," in [*Computer Vision and Pattern Recognition, 2006 IEEE Computer Society Conference on*], **1**, 728–735, IEEE (2006).
[10] Obdržálek, Š. and Matas, J., "Local affine frames for image retrieval," in [*Image and Video Retrieval*], 318–327, Springer (2002).
[11] Phung, S. L., Bouzerdoum, A., and Chai, D., "A novel skin color model in ycbcr color space and its application to human face detection," in [*Image Processing. 2002. Proceedings. 2002 International Conference on*], **1**, I–289, IEEE (2002).
[12] Duman, K., *Methods for target detection in SAR images*, PhD thesis, Bilkent University (2009).
[13] Chang, C.-C. and Lin, C.-J., "LIBSVM: A library for support vector machines," *ACM Transactions on Intelligent Systems and Technology* **2**, 27:1–27:27 (2011). Software available at http://www.csie.ntu.edu.tw/~cjlin/libsvm.
[14] Matthews, B. W., "Comparison of the predicted and observed secondary structure of t4 phage lysozyme," *Biochimica et Biophysica Acta (BBA)-Protein Structure* **405**(2), 442–451 (1975).
[15] Yang, Y. and Liu, X., "A re-examination of text categorization methods," in [*Proceedings of the 22nd annual international ACM SIGIR conference on Research and development in information retrieval*], 42–49, ACM (1999).
[16] Veta, M., Pluim, J. P., van Diest, P. J., Viergever, M., et al., "Breast cancer histopathology image analysis: A review," *Biomedical Engineering, IEEE Transactions on* **61**(5), 1400–1411 (2014).
[17] Cosatto, E., Miller, M., Graf, H. P., and Meyer, J. S., "Grading nuclear pleomorphism on histological micrographs," in [*Pattern Recognition, 2008. ICPR 2008. 19th International Conference on*], 1–4, IEEE (2008).
[18] Bhagavatula, R., Fickus, M., Kelly, W., Guo, C., Ozolek, J., Castro, C., Kovačevi, J., et al., "Automatic identification and delineation of germ layer components in h&e stained images of teratomas derived from human and nonhuman primate embryonic stem cells," in [*Biomedical Imaging: From Nano to Macro, 2010 IEEE International Symposium on*], 1041–1044, IEEE (2010).
[19] Petushi, S., Katsinis, C., Coward, C., Garcia, F., and Tozeren, A., "Automated identification of microstructures on histology slides," in [*Biomedical Imaging: Nano to Macro, 2004. IEEE International Symposium on*], 424–427, IEEE (2004).
[20] Sertel, O., Lozanski, G., Shana'ah, A., and Gurcan, M. N., "Computer-aided detection of centroblasts for follicular lymphoma grading using adaptive likelihood-based cell segmentation," *Biomedical Engineering, IEEE Transactions on* **57**(10), 2613–2616 (2010).
[21] Yorulmaz, O., Oguz, O., Akhan, E., Tuncel, D., Atalay, R. C., and Cetin, A. E., "Multi-resolution superpixels and their applications on fluorescent mesenchymal stem cells images using 1-d sift merging," in [*Image Processing (ICIP), 2015 IEEE International Conference on*], 2495–2499, IEEE (2015).